ACTINIDE RESEARCH QUARTERLY

Actinide Oxides II

Los Alamos
NATIONAL LABORATORY
EST. 1943

The World's Greatest Science Protecting America

Contents
Actinide Research Quarterly

Actinide oxides: the importance of fundamental study

This issue of *Actinide Research Quarterly* continues the discussion of the structure, properties, and reactivity of plutonium dioxide and other oxides. The previous issue focused on recent observations and current understanding of the nature of plutonium dioxide with additional oxygen atoms in the host lattice (PuO_{2+x}). This issue tackles how a strong technical basis ensures the safe and proper stewardship of actinide oxide materials. Articles in both issues are distilled from a series of talks given at a Seaborg Institute workshop held earlier this year on "Actinide Oxides in the Environment, as Stored Material for Nuclear Fuel Fabrication, and in Practical Weapons Components."

We begin this issue with an overview of one of the key drivers for much of this research: the DOE 3013 Standard, which describes how excess plutonium-bearing solids must be processed, packaged, and stored. Kirk Veirs expands on the pragmatic implications of the DOE 3013 Standard in his article about surveillance with observations and historical data on a number of diverse plutonium-bearing materials. Patricia Bielenberg continues the discussion with an article on the practical engineering implications of the storage container in actual use, with an emphasis on the thermal properties of stored plutonium dioxide powder.

In addition to programmatic drivers, this issue delves into the less-explored facets of the thermodynamics of the surface chemistry of plutonium oxide and water. Steve Joyce addresses the uncertainties and fascinating properties of actinide oxides (such as emission of alpha, beta, and gamma particles) in an article about adsorbed water and radiation-driven chemistry. We conclude with an article by Martin Butterfield, Tomasz Durakiewicz, and Rich Martin about additional fundamental details revealed by photoemission spectroscopy coupled with theory of the evolution of several plutonium oxide surfaces following exposure of plutonium metal to oxygen.

These studies contribute to our understanding of the fundamental details of water- and radiation-driven chemistry that occur at the surface of actinide oxides. As discussed in the previous issue, the scientific factors that come into play provide a strong technical basis to ensure the safety and proper stewardship of actinide oxide materials, whether in fabricating nuclear fuel elements, processing materials for long-term storage, or ensuring the integrity of nuclear weapons in the stockpile.

—Mark Paffett

Designing a container for safe, long-term storage
A primer on the DOE 3013 Standard

A crimp-sealed "Food-Pack Can" was used as a convenient packaging arrangement for plutonium-bearing solids not conforming to the 3013

In the decades between the Manhattan Project and the end of the Cold War, the DOE's mission was to support nuclear weapons development and production. Plutonium metal needed to be stored only for short periods before it was recycled into new weapons components. The end of the Cold War and the ratification of the Strategic Arms Reduction Treaties (START) dramatically decreased the needed inventory of nuclear weapons and significantly increased the quantity of special nuclear material being returned to DOE for custody. These excess materials would need longer-term storage.

In collaboration with researchers from Los Alamos National Laboratory, Savannah River Site, and Rocky Flats, the DOE established safety criteria for long-term storage of plutonium materials. In April 1993, the Rocky Flats contractor notified DOE that periodic inspections of stored plutonium metal had not been performed as required. Several concerns were raised: Is this a problem? Is it restricted to Rocky Flats? How should plutonium metal and oxide be stored?

In March 1994 the DOE secretary commissioned a study of plutonium vulnerabilities throughout the complex. The site assessments and evaluations were performed during May and June 1994 with members of the Defense Nuclear Facilities Safety Board serving as observers. The final report, "Plutonium Working Group Report on Environmental, Safety and Health Vulnerabilities Associated with the Department's Plutonium Storage," was issued in November 1994. The plutonium

vulnerability assessment identified numerous storage issues and concerns. It also answered the questions raised at Rocky Flats: Inspecting the stored plutonium metal was a problem, and the problem was not restricted to Rocky Flats.

Consequently, the DOE issued the 3013 Standard in December 1994 and made significant revisions in 1996, 1999, and most recently in 2000. The standard and the container that evolved from it are meant to ensure the safe packaging and storage of plutonium metals and stabilized plutonium oxides for up to fifty years. The current version of the 3013 Standard and container evolved from the need to accommodate changes and refinements in requirements over the last ten years. The original 3013 container as conceived in 1994 was intended to be used both for storage and for transportation. However, by the time the next version of the standard was issued in 1996, the concept had changed so that the 3013 container was to be used only for storage.

The container design and the stabilization requirements in the standard represent a balance between consistently achieving low moisture content in the processed material and containing the resultant "worst-case" pressure. Lower moisture content would reduce the design pressure requirement but would be more difficult to achieve. Higher moisture content might be more easily achieved but would increase the pressure containment requirement dramatically.

Container design: the "safety envelope"
The 3013 Standard addresses design criteria for the "safety envelope" of the containers; requirements for storage facility design, safeguards and security, and transportation are specified in other policies and regulations.

The assembly consists of a minimum of two individually welded, nested containers to isolate
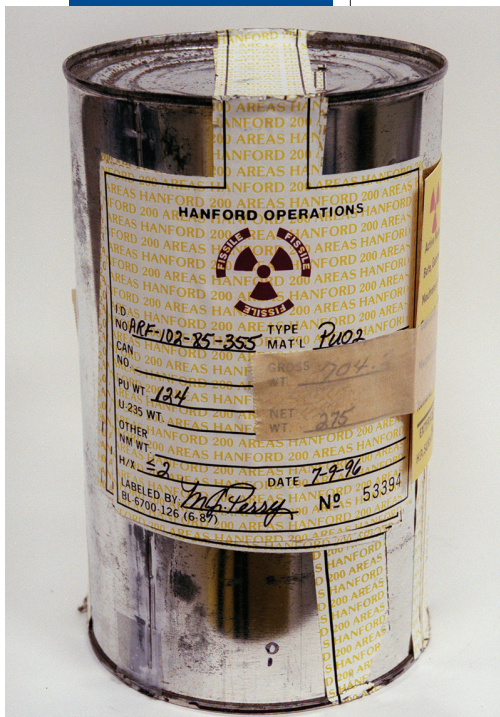
the stored materials from the environment. The outer container provides the pressure boundary to prevent release of the contents. The inner container provides an additional isolation boundary and an internal pressure indicator. Each container is etched or engraved with a unique, permanent identification marking. The storage package has been designed to be maintenance free and compatible with existing or planned qualified shipping containers without the need for additional reprocessing or repackaging.

A sealed container design rather than a container design with a gas filter was selected for two reasons. First, gas filters allow moist air to enter, which could interact with salts and other impurities in the stored materials. Second, if the container was not always oriented properly, stored powder could plug the filters and later "blow out" causing, at a minimum, a local spread of contamination. Full-penetration weld closures provide the highest integrity and longest-life seals possible. Welds eliminate gaskets, which may degrade and leak. Mechanical seals using bolts or screwed connections are susceptible to wear, creep relaxation, seizure, or other mechanical failure. A welded closure is preferred over other closure types because it may provide the

best combination of features such as design qualification test performance, ease of assembly under production conditions in a glovebox, container (package) payload capacity, and achievement of a fifty-year life.

The containers are fabricated of ductile, corrosion-resistant materials, such as 300-series stainless steel (typically 304L or 316L). Typical container dimensions are an inside diameter of 126 millimeters (4.961 inches) and an internal height of 255 millimeters (10.030 inches). The outer container is sized to fit into existing certified or currently proposed shipping containers (primarily the 9975 and SAFKEG packages).
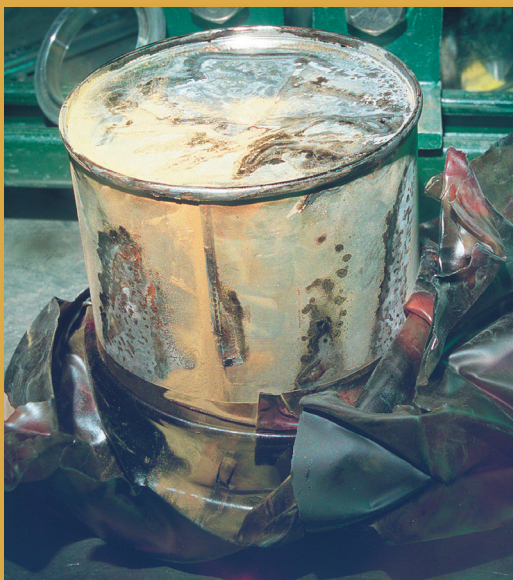
Pre-DOE 3013 Standard packaging of plutonium dioxide in an unopened (left) and partially opened (right) container system. The package was originally prepared at Rocky Flats, shipped to Hanford, and ultimately opened at Los Alamos inside a glovebox at TA-55's PF-4. Note the stage of decomposition of the wrapping tape and materials around the exterior of container.

Criteria for possible damage, change in temperature, and pressurization

The 3013 container design criteria take into account the possibility of mechanical damage, abnormal temperature excursions, and pressurization from a number of mechanisms. A maximum storage height of 30 feet has been set, and the outer container must be able to withstand a drop from that height without releasing any material, that is, it must remain leak-tight. The containers can be used in a range of external environmental conditions, including ambient temperatures up to 52 degrees Celsius (125 degrees Fahrenheit), relative humidity up to 100 percent, and atmospheric pressures down to the equivalent of 8,000 feet above mean sea level.

Conditions are specified for intake air to a storage vault. The vault atmosphere may depart from this specification depending on

Plutonium-bearing solids packaged for analytical work at CMR and awaiting DOT-approved packaging for shipment. These do not conform to the 3013 Standard.

the heat loading in the vault and any facility-specific equipment that may be in use. Containers are loaded in a glovebox with either an inert atmosphere such as nitrogen or possibly argon (as practiced at Los Alamos) or air (as practiced at Hanford).

Facility analyses indicate that loss of cooling isn't uncommon in the operation of a storage vault. The temperature transient depends greatly on the details of the facility system and the ambient conditions, but early estimates were that a container gas temperature as high as 204 degrees Celsius could be reached, which is less than the normal maximum temperatures that might be reached during transportation. Under normal transportation conditions, the average gas temperature within the 3013 container can be as high as 211 degrees Celsius and plutonium metal temperatures might exceed 200 degrees Celsius. This value corresponds to a 3013 container packaged into a 9975 transportation container that is sitting in the sun in an air temperature of 100 degrees Fahrenheit.

The pressure containment function addresses three primary sources of gases that contribute to overall pressurization. These include pressure increases attributed to ideal gas behavior (e.g., the pressure is directly proportional to absolute temperature for a fixed concentration in a sealed fixed volume), helium in-growth due to buildup from the alpha decay of the radionuclides in the package, and pressurization from radiolytically derived hydrogen (or other evolved gaseous species) from water or other species that were initially adsorbed onto the surface of process plutonium (oxide)-bearing solids.

Pressurization analysis assumes that the volume occupied by the gas includes the annular space between the inner and outer containers, the annular space between the inner and convenience containers, the head

space in the convenience container, and the interstitial spaces between the grains of oxide material, including any porosity connected to the container atmosphere. Convenience containers, for instance "Food-Pack Cans," are frequently used to transfer plutonium-bearing material to reduce the potential for contamination. Convenience containers are not required under the 3013 Standard, but if they are used they are placed inside the inner container. No labels are allowed on convenience cans under the 3013 Standard.

Pressurization analysis also considers the effect that material density has on available gas volume. In general, the less pure the oxide material (or the lower the plutonium plus uranium content), the lower the density. As the density is reduced a point is reached at which the convenience container is filled and a minimum gas volume is reached producing the maximum pressure. Further reductions in the contained material density reduce the amount of material that can be loaded into the container, thereby reducing the amount of possible adsorbed moisture available for decomposition and reducing the pressure. (For a more extensive discussion of the pressure

A "Food-Pack Can" has been opened to display its contents inside a glovebox.

design function, see Appendix B of the 2000 revision, DOE-STD-3013-2000.)

Pressure buildup in the inner container for high-purity plutonium dioxide (PuO_2) under normal storage conditions is expected to yield internal pressures of less than 100 pounds per square inch gauge (psig) from all known pressurization mechanisms except water desorption and vaporization. An internal pressure of 100 psig is indicative of unexpected pressurization, yet far below the minimum design pressure of 699 psig for the outer container. The specified design pressure of 699 psig is sufficient to contain the pressure generated by the maximum oxide loading under "worst-case" conditions of 0.5 weight percent (wt %) moisture, 19 watts heat generation, and 211 degrees Celsius (412 degrees Fahrenheit) gas temperature.

One potential for container failure is over-pressurization from a loading error or from an unrecognized gas-generation mechanism. The nested container concept makes it impossible to directly measure gas pressure in the inner container. To overcome this difficulty, the inner container must have a pressure-indicating feature. The most common feature is a deflectable lid, in which changes can be detected by radiography.

Stabilization objectives, packaged materials, and processing conditions

As mentioned earlier, the overall intent of the 3013 Standard is to stabilize excess plutonium-bearing solids and ensure they are secure for up to fifty years. The stabilization objectives include eliminating reactive metal fines (particles in the powder smaller than a specified size) and oxides, eliminating organic materials, reducing water content to below
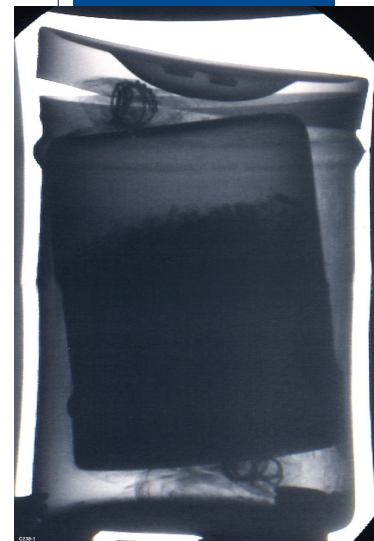
Radiographs of non-3013-packaged solids showing a breach of an outer container (top) and a partial vacuum created in an outer container (bottom) following the reaction of plutonium-bearing material with atmosphere in the sealed containers.

A Primer on the 3013 Standard

0.5 percent by reducing moisture (hydroxyls, hydrates, and adsorbed water), eliminating other gas-producing species, and minimizing moisture uptake after calcination and before sealing in the container.

The standard applies to plutonium-bearing metals and oxides containing at least 30 wt % plutonium plus uranium; there is no lower limit for uranium. It does not apply to materials destined for the Waste Isolation Pilot Plant in southern New Mexico, such as transuranic waste. The standard doesn't limit chloride content, but it recognizes that many materials have significant concentrations of chloride following calcination. Plutonium metals and alloys do not need to be stabilized provided pieces have a mass greater than 50 grams and do not include turnings (or briquettes of plutonium turnings) or wire. Metals must be free of nonadherent corrosion products, liquids, and organic material.

Oxides must be calcined at 950 degrees Celsius for at least two hours and have their stabilization verified by measuring moisture content with a technically appropriate method (loss on ignition for high-purity PuO_2). The defining stabilization criterion is a weight loss of less than 0.5 percent at the time of packaging following calcination. In a 3013 container, the total plutonium or other fissile material mass is less than 4.40 kilogram (kg) with a total mass loading of less than 5.00 kg and a free volume of at least 0.25 liter per kg oxide.

Both the outer and interior containers allow for nondestructive verification, inspection, and surveillance (such as radiography and weighing) of the contents. Storage of plutonium-bearing material must comply with existing materials control and accountability (MC&A), safeguards and security, and audit and surveillance directives, which rely on nondestructive assay as a technique for validation. The MC&A requirements call for routinely assaying stored materials for process, accountability, and inventory controls.

Remaining issues

Although the standard explicitly calls for a surveillance program that captures essential elements, including indication of pressure buildup and weight gain (also indicating leakage), the possibility of corrosion of the container and breach of the container is a technical issue that remains under intensive study. The article on Page 18 discusses observations and a predictive methodology for assessing the lifetime probability of specific 3013 containers. Gas-generation mechanisms arising from simple corrected values for water adsorption/desorption and energetic particle (radiation)-assisted surface chemistry not accounted for in Appendix B (the pressure design function) have recently been identified. Their importance is discussed in the next article.

LANL Assembly

The DOE 3013 nested container system with (from left to right) a British Nuclear Fuels, Ltd., outer container, and an ARIES-designed inner container and convenience can.

Cutaway of the DOE 3103 nested container system demonstrating the fit of the ARIES outer, inner, and convenience containers.

Small-scale containers provide a chance to study many more materials

Gas generation by pure and impure plutonium dioxide materials

Over the last several years, DOE has produced more than 4,500 containers of plutonium-bearing material that meet the requirements of DOE's 3013 Standard. These containers hold approximately 14.0 metric tons of metal, oxide, and impure oxide (30 weight percent or greater of plutonium plus uranium). The packaging configuration specified by the standard consists of robust, nested, welded containers with a minimum design pressure of 699 pounds per square inch gauge (psig). This is in contrast to interim storage containers in use at TA-55 designed by Roland Hagan that are fitted with filters to allow "breathing," or to crimp-sealed cans, which can withstand only minor internal pressures. Gases generated by the material over the fifty-year-allowed storage lifetime will remain within the container and could lead to pressurization and corrosion of the packaging.

The DOE 3013 Standard specifies a set of robust, nested, welded containers. Shown are the British Nuclear Fuels, Ltd.-designed outer, inner, and convenience containers.

During the development of the current 3013 Standard, there was limited information concerning gas generation from actual plutonium-bearing materials. It was assumed that the only mechanisms for gas generation were the production of helium from alpha decay (a minimal source of gas) and radiolysis of water. It was also assumed that all of the water in the container would radiolyze to hydrogen gas and the oxygen from the radiolysis of water would be taken up by the material.

The lack of oxygen in the gas-phase reduces the hazard of the system in two ways. First, the overall pressure from radiolysis of water is reduced by a third, one mole of hydrogen for every mole of water rather than one mole of hydrogen and a half mole of oxygen for every mole of water. Second, the possibility of a flammable mixture within the container is removed. These assumptions were based on a handful of experiments and extensive experience throughout the DOE complex with plutonium-bearing materials. However, the gas-generation behavior of materials that are actually being packaged had not been studied.

During the last two years, Los Alamos' Surveillance and Monitoring Program (formerly the 94-1 Program) has studied the gas-generation

Gas Generation

Top: A small-scale container is shown beside a large-scale container. Bottom: Forty-five of the small-scale containers are assembled in an array.
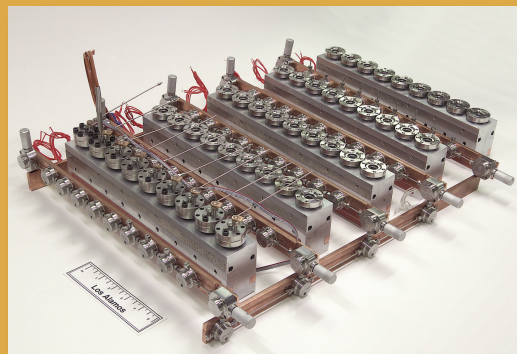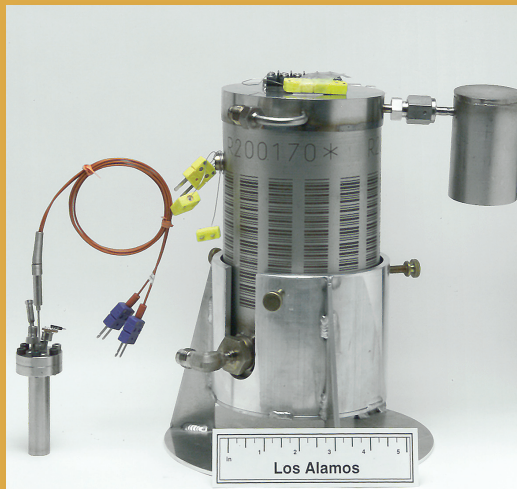
behavior of materials provided by Rocky Flats Environmental Technology Site (RFETS), Hanford, and Los Alamos, which are representative of the classes of materials that have been packaged by sites across the DOE complex. Large-scale instrumented containers that can hold five kilograms (kg) of material within a 2.38-liter internal volume were made by modifying a British Nuclear Fuels, Ltd. (BNFL) inner container to include a Raman spectroscopy chamber, thermocouples, pressure sensor, corrosion sensors, and a gas manifold to extract samples for gas chromatography or mass spectrometry analysis. These containers are meant to provide conditions as close as possible to the conditions experienced by materials packaged under the 3013 Standard.

Because of the size of the containers and the amount of material needed, only a limited number of studies are planned using the large-scale containers. An array of 45 Los Alamos-designed, small-scale containers, scaled to 1/500th the volume of the BNFL 3013 inner container, or 5 milliliters, provides a chance to study many more materials and to vary the moisture content. Results from these small-scale containers are compared to the large-scale container results to verify that they are applicable to packaged materials. The pressure of each small-scale container and the temperature of the heated block that holds it are monitored continuously. Each heated block contains nine small-scale containers and the temperature of each of the five blocks, which is held constant by a controller, can be varied independently. Each small-scale container has a 45-microliter sampling loop that provides the capability of gas composition analysis using a gas chromatograph.

Gas generation by pure oxides

A high-purity plutonium oxide material was studied in both the large- and small-scale containers. This material contained 87.8 percent plutonium with 0.15 percent identified impurities (stoichiometric PuO_2 of this purity and isotopic composition should be 88.1 percent), had a specific surface area of

A high-purity plutonium oxide material was studied in the large- and small-scale containers.

1.08 square meters per gram (m^2/g), and a pycnometer density of 11.5 grams per cubic centimeter (g/cm^3). This material is a very fine brown powder.

Five kilograms of high-purity plutonium oxide were calcined to 950 degrees Celsius, and the freshly calcined material was sealed in a large-scale container with pure helium as the fill gas. The temperature, pressure, and gas composition were monitored for 469 days. No change in the gas composition was observed. Neither hydrogen nor oxygen was detected; the only gas observed within the container was helium. The pressure increased by only 0.3 kilopascal (kPa). The majority of the helium from alpha decay of the plutonium apparently remained trapped within the oxide particles. The amount of helium from alpha decay would have been sufficient to raise the pressure by 1.2 kPa had all of the helium entered the gas phase.

The material was then exposed to a flow of humidified helium gas—60 percent relative humidity at 25 degrees Celsius (with a water-vapor pressure of about 1.9 kPa)—for 24 hours. The material picked up 1.25 grams of water—0.025 weight percent (wt %), which is equivalent to one monolayer of water. The fill gas was changed to helium with about 10 percent air to reproduce the conditions experienced by containers being packaged at RFETS. Under these starting conditions, we initially observed nitrogen, oxygen, and water in addition to helium as the gas composition of the fill gas. The water was observed by Raman spectroscopy—gas chromatography (GC) analysis using our instrumentation does not detect water. Oxygen was depleted to below detection limits within twenty-five days. The water in the gas phase, which is a small fraction of the water added to the container, decreased by about half and remained at a steady partial pressure for more than one hundred days. No hydrogen gas was observed.
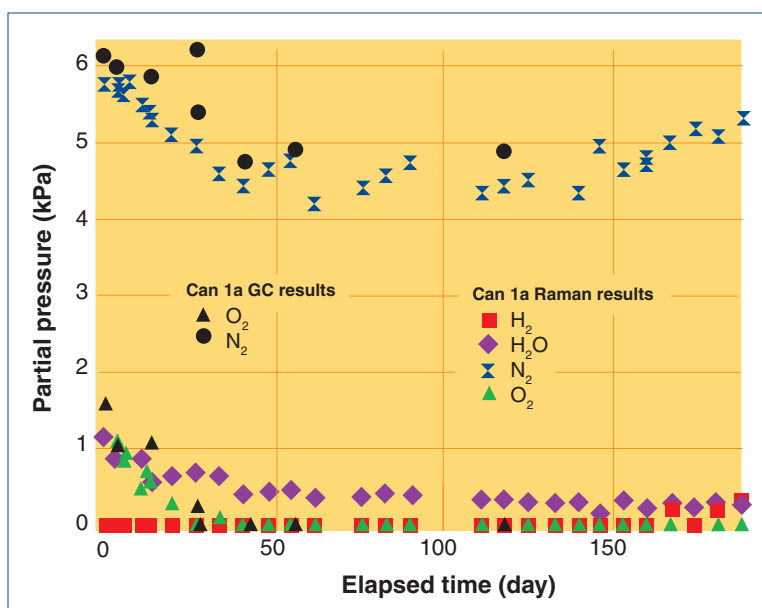
The calcined high-purity plutonium oxide material was also used for studies in the small-scale containers that started about one year after the large-scale containers were

High-purity PuO_2			
	CO_2	N_2O	H_2
First five days			
No added H_2O	0.28	0.04	0.02
0.5 wt % added H_2O	0.62	0.58	0.13
2 wt % added H_2O	0.49	0.40	0.10
Next 31 days			
No added H_2O	0.04	-0.00	0.01
0.5 wt % added H_2O	-0.00	0.01	0.20
2 wt % added H_2O	0.08	0.04	0.28
Next 12 days			
No added H_2O	0.04	0.00	0.01
0.5 wt % added H_2O	0.08	0.02	0.29
2 wt % added H_2O	0.08	0.02	0.37

Rates of gas generation in units of kilopascal per day for carbon dioxide (CO_2), nitrous oxide (N_2O), and hydrogen (H_2).

Can 1a GC results
▲ O_2
● N_2

Can 1a Raman results
■ H_2
◆ H_2O
✕ N_2
▲ O_2

Results of experiments on gas generation by high-purity plutonium dioxide exposed to humidified helium are shown at left.

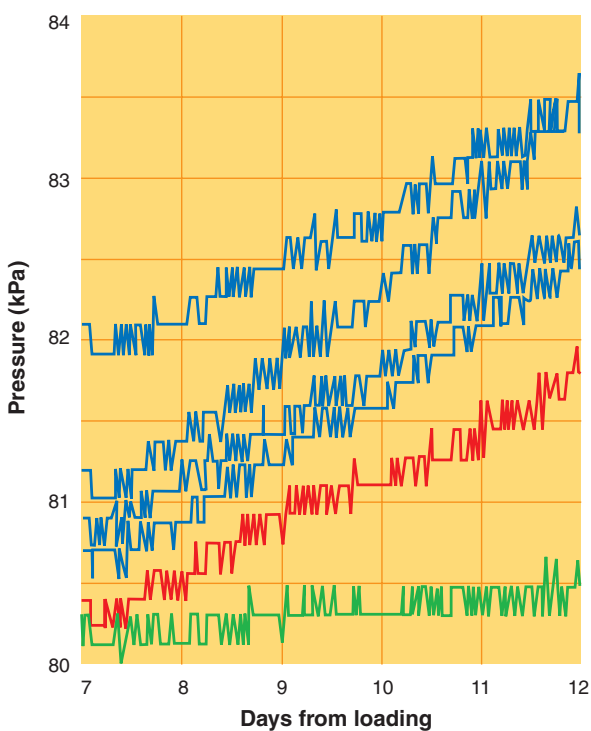loaded. The material was exposed to the dry glovebox atmosphere during that time. The material apparently adsorbed atmospheric gases during that time. We studied high-purity plutonium oxide with no water added, with 0.5 wt % added water, and with 2.0 wt % added water. The starting material would have picked up some water during its one-year exposure to the glovebox atmosphere. The amount of water in the starting mate-rial is not known but is expected to be less than 0.1 wt %.

Several gaseous species were pro-duced under these conditions that were not seen in the large-scale studies. Gas chromatography analysis of the fill gas immediately after the reactors were sealed showed mainly heli-um with nitrogen and oxygen and barely detectable hydrogen. Within five days, gas chromatography analysis of the fill gas shows CO_2, N_2O, and H_2 present in quantities well above the sensitivity of the GC. Interestingly, during the first five days, the gas-generation rates for CO_2 are substantially larger than the gas-generation rate of H_2 regardless of the amount of water added to the container. Nitrous oxide is pro-duced at the second fastest rate in the first five days. For the containers with water added, the rate of N_2O production is slightly less than the rate of CO_2 production, both of which are larg-er than the H_2 gas-generation rate by a factor of

4 to 5 times greater. When water is not added to the container, the rate of N_2O production is smaller by a factor of 10 as compared to the containers with water added yet is still larger than the hydrogen gas-generation rate when no water is added. Hydrogen is generated at the slowest rate during the first five days.

During the next thirty-one days, the overall gas-generation rate decreases because the CO_2 and N_2O rates decrease substantially to about 10 to 20 percent of what they were in the first five days. The H_2 rate increases during this time for the containers with water added and decreases in the containers with no added water. Gas-generation rates of 0.05 kPa/day or less are difficult to measure, so the rates reported will have an error of approximately that magnitude. The next twelve days show very little change in the gas-generation rates from days six to thirty-seven. The H_2 gas-gen-eration rate in the containers with added water seems to increase, but this is probably due to measurement errors.

The pressure versus time (PVT) of the containers for the sample with no water added (green curve), four samples with 0.5 wt % wa-ter added (blue curves), and one sample with 2.0 wt % water added (red curve) is shown at left. The curve for the container with no water added is easily distinguished from the curves of the containers with added water. The curve for the container with 2.0 wt % added water appears quite similar to the curves for the containers with 0.5 wt % water added. The curves were adjusted for clarity to be on the same scale and slightly offset by adding a constant value to the pressures.

The observation that H_2 gas-generation rates are very similar if not the same for pure oxides with 0.5 and 2.0 wt % added water is best explained by considering how much water the material can reasonably absorb. A pure plutonium oxide particle will adsorb water onto its surface until the surface is

Pressure versus time of the contain-ers for pure pluto-nium oxide samples with no water added (green curve), 0.5 weight percent water added (blue curves), and 2.0 weight percent water added (red curve).

saturated, which occurs at three to five mono-layers when the particle is exposed to a high relative humidity atmosphere. One monolayer of water on high-purity plutonium oxide with a specific surface area of 1.08 m^2/g occurs at about 0.025 wt %. Saturation of the surface with water will start to occur at about 0.1–0.2 wt %. Additional water added to the container will seek the coldest part of the container, which in this case is not the plutonium oxide because it self heats. Thus, the containers with 0.5 and 2.0 wt % added water will behave similarly because the extra water is condensed away from the plutonium oxide and not ex-posed to significant alpha radiation. This is not the case for impure oxides containing salts.
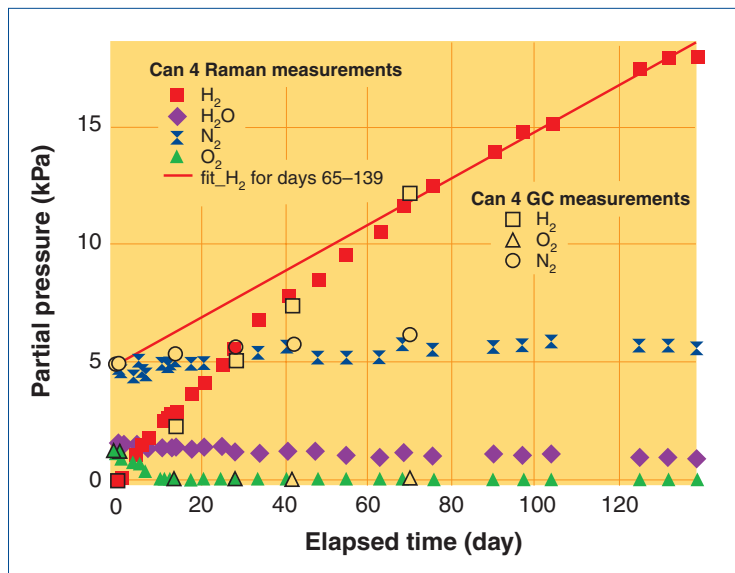
Gas generation by impure oxides

Typical Los Alamos impure oxide materi-als in the packaged 3013 containers contain plutonium oxide with salt mixtures of sodium chloride (NaCl), potassium chloride (KCl), and magnesium chloride (MgCl$_2$). We have studied salt-containing materials in both the large- and small-scale containers. The salt-containing material in the large-scale container was pro-duced by combining burned anode heals and electrorefining salt residues for a blend that would have sodium and potassium chloride salts with a trace of magnesium chloride salts. This material was calcined at 800 degrees Celsius for two hours.

Water was added by flowing humidified helium (with a water-vapor pressure of approximately 2.3 kPa) through the container from the bottom to the top. The material gained 8 grams of water (0.19 wt %) after 24 hours. Hydrogen was generated and oxygen was depleted. Water was seen in the gas phase, indicating that the salts were in equilib-rium with the water vapor. The initial hydro-gen gas-generation rate was 0.19 kPa/day.

Researchers in Los Alamos' Materials Identification and Surveillance (MIS) Program received from Hanford a low-purity plutoni-um-bearing salt with 70.0 percent plutonium,

Results of experiments on gas generation by impure oxides.
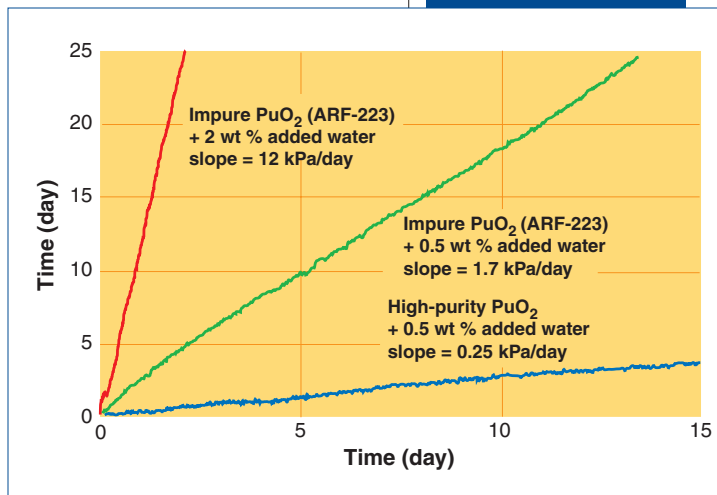
Comparison of the pressure versus time curve for two impure oxide samples and one high-purity sample.

GAS GENERATION

Gas pressure in kPa in the headspace of small-scale containers with impure PuO_2			
Added water	0.0 wt %	0.5 wt %	2.0 wt %
He	60	65	44
H_2	1	37	173
O_2	2	1	22
N_2	43	16	17
N_2O	0	3	3
CO_2	1	0	0
CO	1	1	1

G-values	
Material	G_{H2} (molecules/ 100eV)
High-purity PuO_2	0.9–1.7
Impure PuO_2 (Hanford)	2.5–3.8

5.5 percent chlorine, 1.9 percent potassium, 1.5 percent sodium, and 0.5 percent magnesium. Seven samples were studied in small-scale containers: one with no added water, five with 0.5 wt % added water, and one with 2.0 wt % added water. In contrast to the pure oxide material, there were large differences in the gas-generation rates of samples with different amounts of added water. In addition, at the higher water loading, oxygen was generated as well as hydrogen.

A comparison of the pressure versus time curve for the impure PuO_2 salt (Hanford) samples and one of the pure oxide samples shows that the salt materials generate gas more rapidly than the pure material. Analysis of the gas composition reveals that the pressure rise for the impure PuO_2 salt sample with 0.5 wt % water added is composed of hydrogen gas generation and oxygen gas depletion. The pressure rise for the impure PuO_2 salt sample with 2.0 wt % water added was caused by both hydrogen and oxygen gas generation. The hydrogen gas-generation rates obtained from gas analysis for these two samples are 5.1 and 5.7 kPa/day when normalized to 1 wt % added water.
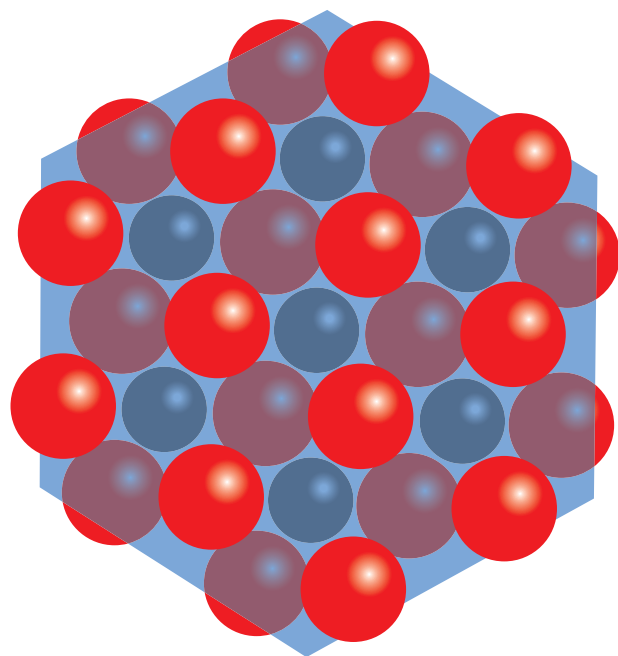
Analysis of the gas constituents for the small-scale containers with impure PuO_2 salt at two weeks shows that oxygen is depleted in the containers with 0.5 wt % added water or less but that oxygen is generated in the container with 2.0 wt % added water.

The ratio of hydrogen to oxygen decreases from about 8 to about 4 at longer times. At these ratios the gases are flammable.

Gas-generation rates in terms of pressure over time are of interest to regulators and managers of storage facilities because they can readily understand how and if containers pressurize. In radiation studies on hydrogen containing materials the usual unit for providing a rough estimate of gas generation is the G value. The rate of radiolysis (e.g., the G value,) is thus defined as the number of H_2 molecules produced with every 100 electron-volts (eV) of absorbed energy.

G values can be derived from our data using the volume of the containers, the density of the material, the amount of material, and the increase in pressure. There are a number of methods of determining the G value and can include elaborate geometrical models of how the water is distributed on the plutonium dioxide and associated materials. Regardless of the simplifying assumptions used, the values determined in our studies can be compared to G values reported recently in the literature: for pure water $G_{H2}=1$, for magnesium chloride hexahydrate exposed to gamma radiation $G_{H2}=0.1$, and for pure plutonium dioxide powder exposed to a high-humidity atmosphere $G_{H2}= 1.1$ to 8.6.

These empirical observations clearly indicate the high variability in gas generation from pure and impure plutonium-bearing materials. Furthermore, pragmatic implications of these studies also provide guidance on which stored material types need more extensive surveillance. The later aspect is an explicit requirement stated in the DOE 3013-2000 Standard.

Chemistry at the interface

Exploring thermal- and radiation-induced interactions of water on uranium dioxide surfaces

Most plans for the disposition of surplus and waste nuclear materials involve storage in sealed containers where the evolution of gases from reactions of adsorbed species, most notably water, can present both pressure and flammability hazards. Despite efforts such as calcining the material and handling in "dry" gloveboxes to minimize the water content before packaging, both residual moisture and readsorbed water are likely to be present in the final containers. Given the anticipated temperature excursions during transportation and storage, this water may thermally desorb, increasing the pressure, or thermally dissociate to produce hydrogen (H_2) gas, increasing flammability hazards. In addition, radiation from the nuclear material may induce radiolysis of the water both in the gas phase and in the adsorbed state with likely products being H_2, oxygen (O_2), and hydrogen peroxide (H_2O_2).

For high-surface-area samples such as those typical of the materials disposition programs described in the article by Kirk Veirs on Page 7, the overwhelming majority of the water would be in the adsorbed state. Predictive modeling over the storage lifetimes of such containers requires understanding the thermal- and radiation-induced chemistry that occurs in multiple phases (gas, solid, and interface). There has been considerable study of the radiolysis of the homogeneous phases of water. For the heterogeneous adsorbed state, the sparser existing literature indicates that significant changes in radiolysis yields and product distributions can occur. To better understand the relative importance of the thermal- and radiation-induced chemistry, we have studied the interactions of water on single crystals of uranium dioxide (UO_2) where the experiments have been designed to specifically address the issues of chemistry at the interface.

All of the studies presented here were conducted using single-crystal samples of uranium dioxide in an ultrahigh vacuum environment. Currently only thorium dioxide (ThO_2) and uranium dioxide are available as macroscopic single crystals of the actinide oxides. Such an approach offers a number of advantages for understanding the fundamental mechanisms of the interactions of water with actinide oxide surfaces. Single crystals, prepared and characterized using

Normal view of the UO_2 (111) surface. Red spheres are oxygen; black spheres are uranium. The blue hexagon is the plane through the uranium atoms and indicates the three-dimensional nature of the surface.

standard surface analytical techniques, have well-defined structures and compositions with minimal defects, making them ideal for molecular-level studies.

Uranium dioxide, as with many of the actinide dioxides, adopts a fluorite lattice, where uranium is formally U^{4+} and eight-fold coordinated and oxygen is formally O^{2-} and four-fold coordinated. The (111) fluorite surface, used for most of the studies discussed here, is composed of one seven-fold uranium and two three-fold oxygens. This surface is stoichiometric, nonpolar, and formed by cleaving the fewest bonds. The (111) is the lowest-energy termination and does not reconstruct—meaning the surface atoms are essentially in locations consistent with an ideal termination of the bulk lattice—whereas for higher-energy surfaces such as the (100) and (110) the surface atoms often rearrange to lower the overall free energy. As such, studies of the (111), with its known geometric structure, are ideal for comparisons between experiment and theory.

In addition to the obvious benefits of preparing, characterizing, and maintaining clean samples, working in ultrahigh vacuum also aids in isolating the elementary chemical steps in the thermal- and radiation-induced

chemistry of water on surfaces. The absence of a gas phase, except during precisely controlled exposures, minimizes the effects of readsorption, which can greatly complicate kinetic analyses. Vacuum also eliminates any contributions from gas-phase radiolysis.

Temperature programmed desorption (TPD) was the principal experimental technique used to investigate the thermal chemistry of water on uranium dioxide surfaces. In TPD, the surface is exposed to controlled quantities of water at low temperatures, the surface is then heated, and gaseous product evolution is monitored with a mass spectrometer. Evolved gas-phase products are directly determined and binding energies and reaction kinetics can be obtained from an analysis of the desorption temperature profiles. Essentially, the more strongly bound a species, the higher the temperature required to desorb it.

The TPD results for clean, minimally defected uranium dioxide surfaces, exposed to deuterium oxide (D_2O), are relatively straightforward. The only desorbing species is water; we didn't detect any deuterium gas (D_2), O_2, or other species that would indicate a dissociative adsorption of water. Two distinct states for adsorbed water were observed: low-temperature nonsaturating, and high-temperature saturating. The low-temperature nonsaturating state can be attributed to the formation of condensed multilayers of water on the surface with a binding energy of 11 kilocalories per mole (kcal/mole) consistent with the sublimation of water ice. The high-temperature saturating state can be attributed to the direct interaction between water and the uranium dioxide surface. A simple kinetic analysis of this monolayer state yields a binding energy of approximately 13–15 kcal/mole. This value compares favorably with both ab initio electronic structure calculations and
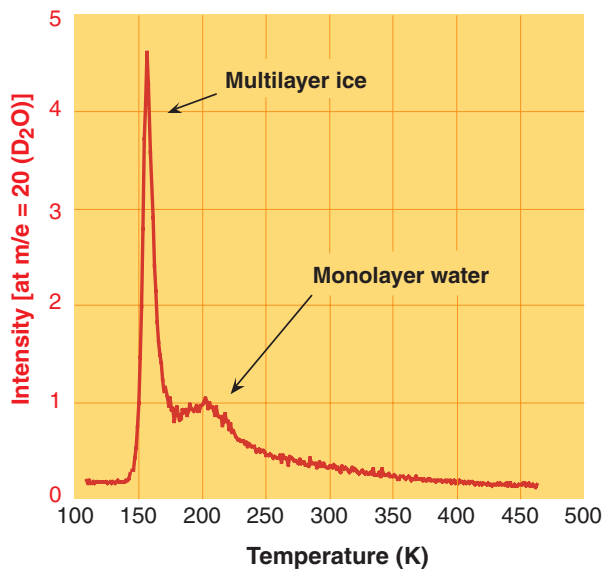

The thermal desorption of adsorbed deuterium oxide (D_2O) from uranium oxide (UO_2) (III).

experimentally determined binding energy of water with isostructural plutonium dioxide.

The TPD results indicate that the majority of water interacts molecularly on clean uranium dioxide (111) surfaces with a binding energy only slightly greater than water with itself. However, this small change can have important implications in "real-world" environments. A steady-state kinetic model can be used to determine the vapor pressure of water needed to form the direct, monolayer film. Based on the TPD-derived binding energy of 13–15 kcal/mole, a water pressure of only a few millitorr is enough to saturate the monolayer film at room temperature. This pressure is below that used in most gloveboxes, so most processed material will, except in the driest boxes, readsorb one layer of water. Most of the standards developed for nuclear materials storage require accounting for at least this level of water loading when designing the containers.

In addition to the thermal chemistry of the actinide oxides, there exists the potential for radiation-induced chemistry—or radiolysis. All of the isotopes of the actinides are radioactive and thus can emit a variety of particles and ionizing radiation including alpha (α), beta (β), and gamma (γ) particles; neutrons; recoil and fission atoms; and secondarily produced electrons, ions, and x-rays. These decay particles, for example, the approximately five-million-electronvolt (MeV) α typical of the more common actinides including uranium-238 and plutonium-239, transfer their considerable energy to the surrounding media, inducing reaction and displacing atoms. The short-lived primary radiolytic products such as ions, electrons, atoms, and free radicals initiate further ion-molecule and free-radical reactions ultimately leading to more stable radiolysis products. These final radiation-induced products are often quite distinct from the thermal chemical products.

While the objective is to understand the radiation chemistry that occurs at the surfaces of radioactive materials, there are practical and scientific advantages to using external radiation sources on either low-activity or surrogate substrates. Time and safety issues are the most obvious. For a modestly active material such as plutonium-239, approximately 10,000,000
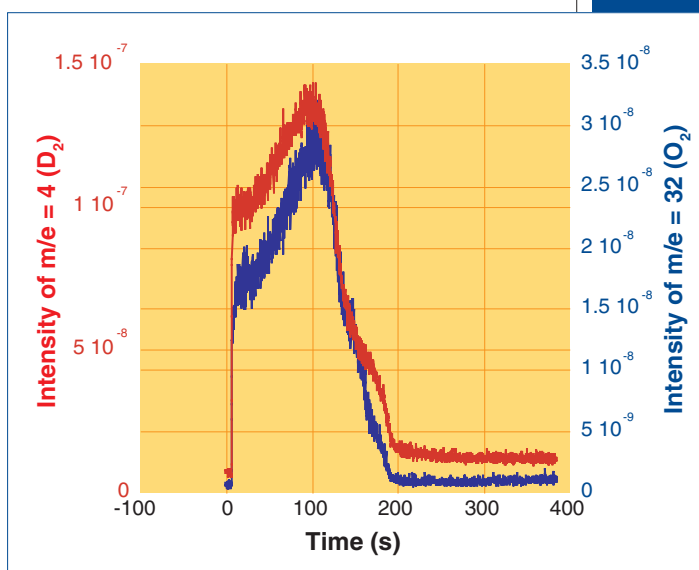
alpha particles traverse a square centimeter of surface per second. Assuming ten radiolytic events at the surface per alpha particle, it would take 10,000,000 seconds (about four months) to convert a monolayer (approximately one quadrillion sites per square centimeter). While relatively short compared to storage timescales, this time is inconveniently long for most laboratory studies.

By necessity, high-surface-area materials are typically used to increase signals when relying on the intrinsic radioactivity. Electron guns and ion beams have currents ranging from nanoamps to microamps with typical beam sizes on the order of several millimeters allowing for monolayer conversions in seconds to hours. This accelerated

The evolution of deuterium gas (D_2) and oxygen (O_2) following electron irradiation of deuterium oxide (D_2O)-covered uranium dioxide (UO_2) (III).

Exploring Interactions

For further reading:

"The Interactions of Water with Solid Surfaces: Fundamental Aspects Revisited," M.A. Henderson, Surface Science Reports, 46, 1, 2002.

"A Critical Examination of the Thermodynamics of Water Adsorption on Actinide Oxide Surfaces", M.T. Paffett, D. Kelly, S.A. Joyce, J. Morris, K. Veirs, Journal of Nuclear Materials, 322, 45, 2003.

rate allows for the use of planar, single-crystal substrates. Alpha particles lose more than 99 percent of their energy to the surrounding media by ionization events and the production of secondary electrons. The mean energy of secondary electrons is on the order of 100 electronvolts (eV) with approximately 10,000 secondary electrons produced per alpha decay event. The alpha produces only about 200 lattice-atom displacements; the majority of the lattice damage, more than 2,000 displacements, results from the recoil atom—a 70 kiloelectronvolt (keV) thorium-234 for uranium-238. Both ionization and displacement effects can be simulated by using convenient low-energy laboratory sources.

Low-energy electrons, 100–500 eV, were used to simulate the ionization-induced chemistry of water adsorbed on uranium dioxide surfaces. The primary radiation-induced products are D_2 gas, O_2 gas, and small amounts of water. The absolute and relative amounts of D_2 and O_2 produced are functions of the temperature and coverage of water. The highest yields occur for multilayer water. D_2 is produced in hyperstoichiometric amounts—for example, the $D_2:O_2$ ratio is at least 5; ideally it would be 2 for D_2O (deuterium oxide or heavy water). The cause of the oxygen deficiency in the neutral products is poorly understood.

Hyperstoichiometric hydrogen production (with respect to O_2) is observed in the radiolysis of pure gas- and liquid-phase water. In these cases, the oxygen balance is maintained through the formation of H_2O_2. No peroxide gas evolved during irradiation although small amounts were retained in the multilayer ice as observed during TPD following irradiation. For monolayer and lower coverage, the overall yields decreased, but the $D_2:O_2$ ratio actually increased (exceeding 10). No peroxide was observed for monolayer coverages. Although we are awaiting more definitive experiments, it is likely that some of the "missing" oxygen

becomes incorporated into the uranium dioxide substrate.

In addition to neutral species, positive ion desorption during irradiation was monitored as well. For a nominally clean uranium dioxide surface, electron irradiation yielded oxygen (O), hydrogen (H), and fluorine (F) cations. The H^+ came from the small adsorption of water from the background gases in the system, and the F^+ was attributed to impurities in the fluxes used to produce the uranium dioxide crystal. This result highlights the potential sensitivity of ion desorption to minority low-concentration species. A D^+ ion was the only species observed from multilayers of water, which is consistent with previous work (heavy water was used to distinguish between traces of background water in the vacuum chamber).

For submonolayer amounts of water, D^+ and OD^+ were the primary products. The D^+ and OD^+ signals persisted to surface temperatures up to 600 kelvin (K). From the thermal studies discussed above, all molecular water was observed to desorb by 300 K. To determine the origin of the OD species, isotopically labeled ^{18}O was incorporated into the surface by ion sputtering. Upon exposure to $D_2{}^{16}O$, ^{18}OD ions were observed, indicating that at least some of the oxygen comes from the substrate as the result of dissociation of water at minority defect sites not observed in the TPD studies.

The observation of OD^+ suggests that defects on the uranium dioxide surface could have a dramatically different chemistry than the majority sites. To further explore this, we intentionally introduced defects into the surface by low-energy argon (Ar) ion sputtering. Ion bombardment of surfaces produces numerous defects at the surface and the near-surface region. In addition to the sputtered surface species, which yield surface vacancies, the collisional cascade creates lattice defects such as vacancy or interstitial (Frenkel) pairs.

The collisional cascades created by 5 keV Ar^+ ions are very similar, differing principally in extent, to those produced by a recoil atom. In compounds, preferential sputtering of one element is often observed. In general, lower-mass species are more likely to be sputtered. For metal oxides, the preferential sputtering of oxygen becomes more pronounced as the metal becomes heavier. For uranium dioxide, oxygen depletion of the near-surface region has been observed using x-ray photoelectron spectroscopy (XPS) after ion bombardment.

TPD experiments were performed for both annealed (minimal defects) and sputtered (highly defected) uranium dioxide surfaces following exposure to heavy water. Significant deuterium gas desorption was observed above 400 K for the defective surface but was not observed for the annealed surface. The hydrogen evolution from the defective uranium dioxide surface likely resulted from the dissociative adsorption of heavy water at defect sites to form adsorbed hydroxyls. There were no other high-temperature desorption peaks observed at m/z (mass-to-charge ratio) 20 or 32 to suggest that there is a high-temperature reaction that leads to the gas-phase evolution of a product containing the oxygen from the water. This oxygen could, therefore, remain at the surface and heal the defects that lead to D_2 gas generation.

To provide experimental evidence of the reoxidation of the sample by water, TPD experiments were performed for successive heavy-water exposures to the sputtered sample surface. To minimize thermally healing the defects, the TPD heating ramp for this series of experiments was terminated at 500 K, at which point the majority of D_2 gas had desorbed but was still about 200 K lower than where the defects were observed to be thermally annealed. After the first heavy-water dose there was a significant decrease in the amount of hydrogen desorption for the second and subsequent exposures. After five exposures, the TPD for the sputtered and annealed surfaces were indistinguishable. Water therefore can heal defects, presumably oxygen vacancies, with the attendant evolution of hydrogen gas.

The irradiation results indicate that over prolonged periods, significant radiolytic production of H_2 and O_2 can occur. In all cases, H_2 was produced in excess of O_2, which is consistent with previous work on gas generation from plutonium dioxide powders. As the absolute yields decrease and relative H_2:O_2 yields increase with decreasing water loading, these results suggest that minimizing moisture content would be beneficial not only in reducing the pressure hazards, but also in ensuring that the gas composition is outside the flammability limits for hydrogen and oxygen mixtures. We have also identified an additional channel for hydrogen production: surface defects. Because the damage resulting from ion sputtering is similar to that caused by the recoil atom formed during radioactive decay, the thermal chemistry at defects may be an indirect but significant factor in the radiation chemistry of adsorbed species on alpha-emitting materials.

The thermal desorption of deuterium gas (D_2) following deuterium oxide (D_2O) exposure to sputter-damaged uranium dioxide (UO_2) (III).
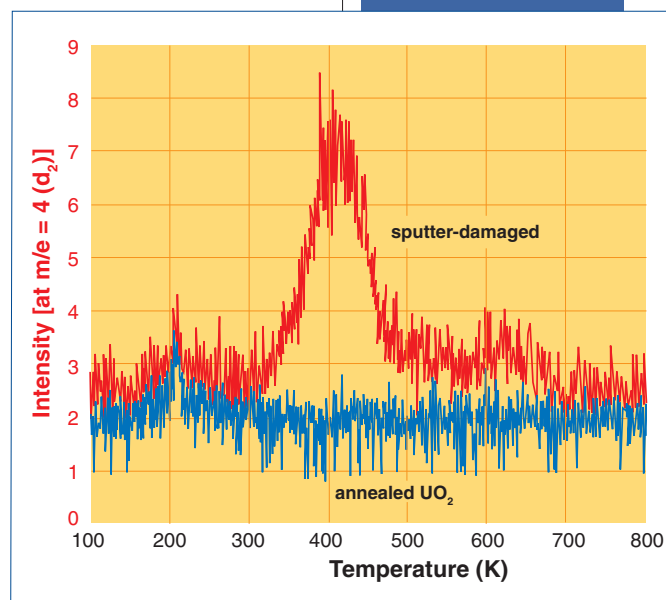
Temperature has a direct effect on pressure and corrosion in the 3013 container

Modeling the thermal conductivity of fine plutonium dioxide powder

This article was contributed by Patricia Bielenberg with significant contributions from Kirk Veirs, John Berg, Dennis Padilla, Alex Carrillo, and Laura Worl, all of Nuclear Materials Technology Division; and David Harradine, Chemistry Division. Principal developers of the model are Coyne Prenger, Engineering Sciences and Applications Division, and Jerry Jones, Villanova University.

For further reading:

"Thermal Analysis of the 9975 Package with the 3013 Configuration as a Plutonium Storage Container," S.J. Hensel, Westinghouse Savannah River Report, WSRC-TR-98-00420, 1998.

"Thermal Analyses of Putonium Materials in Stainless Steel Containers," T. Knight and R. Steinke, Transactions of the American Nuclear Society, 1997.

The thermal properties of the 3013 storage container plus plutonium bearing materials are fundamental to understanding behavior during storage and transportation. For instance, as the temperature increases, outgassing in the container, fill-gas pressure, and water vapor pressure all increase. Changes also occur in the distribution of water between solid phases such as salt, oxide, and container walls and the kinetics of reactions affecting hydrogen gas generation and corrosion. Because of the direct effect that temperature has on pressure and corrosion in this sealed material-storage system, an accurate analysis is needed to correctly anticipate these effects.

Two extensive thermal analyses have been carried out on 3013 containers holding pure plutonium dioxide (PuO_2) powders. Both studies were limited by the lack of information available for plutonium dioxide powder thermal conductivity, which controls the thermal behavior in these containers. One study, reported in 1997 by Thad Knight and Robert Steinke of Los Alamos, used the Deissler-Eian correlation for packed beds to estimate the powder thermal conductivity as a function of the porosity and the gas and solid thermal conductivities. They predicted that the thermal conductivity for a plutonium dioxide powder with a porosity of 74 percent at 100 degrees Celsius in air was equal to 0.10 watt per meter kelvin, or W/(m K). In the second study, reported in 1998, Steve Hensel of Savannah River Site estimated that the oxide powder in air had a constant thermal conductivity of 0.079 W/(m K), but no information was provided on how this estimate was made. These two estimates of the powder thermal conductivity differ by 20 percent.

In an effort to decrease the uncertainty in the current temperature-profile predictions for the plutonium dioxide powder beds, experimental measurements were made of the thermal behavior of pure plutonium oxide powder over a wide range of pressures—0.05 to 334 kilopascals (kPa)—with two different fill gases: argon and helium. In addition, an analytical thermal conductivity model was developed to aid in the analysis of the experimental data and to provide predictive capabilities. The model uses the porosity, pore size, interstitial gas pressure, and the thermal conductivities of the gas and solid to calculate the thermal conductivity of the powder. With the new model, the previous

Thermocouples are placed along the diameter of a British Nuclear Fuels, Ltd. (BNFL) 3013 container about 2.5 inches from the bottom. The container is filled with 5 kilograms of plutonium dioxide powder, which extends to within 1.5 inches of the top of the container. Additional thermocouples were located on the outside of the container for measurement.

predictions of the thermal profiles in the container can be compared and assessed.

Experimental thermal measurements

Thermal conductivity measurements were performed on a plutonium-239 dioxide bed in a cylindrical stainless steel container equipped with ten thermocouples located radially across the container for temperature profile measurement. The container was loaded with 5.0 kilograms (kg) of plutonium dioxide with a porosity of 77.4 percent and a constant heat generation rate of 2.06 watts per kilogram (W/kg). Because the powder generates heat, it provides a constant heat source. After about four hours, a steady-state temperature profile is achieved and measured.

Helium and argon were used as fill gases because of the large gas conductivity range (thermal conductivities for helium and argon are 0.16 and 0.018 W/(m K) at 27 degrees Celsius, respectively). Typically, at higher gas pressures (greater than 10 kPa), the powder thermal conductivity is controlled by the gas thermal conductivity, so significant differences in the powder thermal behavior would be expected with these two gases.

When plotting the effects of pressure and fill gas on the centerline temperature in the plutonium dioxide bed, it was noted that the centerline temperature increased with decreasing pressure. This effect arises because the gas transitions from the continuum limit to the free molecular flow limit where the gas thermal conductivity is proportional to the pressure. At the lowest pressures used in this study (less than 0.1 kPa), the powder conductivity becomes independent of both pressure and fill gas because solid-solid conduction and thermal radiation pathways are the dominant contributors to temperature in the bed.

At higher pressures, the powder thermal behavior does not scale with the fill-gas thermal conductivity as initially hypothesized.

From the temperature profiles the estimated powder thermal conductivities at 82 kPa for argon and helium are 0.077 and 0.22 W/(m K), respectively. The powder thermal conductivity with helium as fill gas is only three times that with argon as fill gas. This was surprising because the helium gas thermal conductivity is nine times that of argon under these conditions. These results indicate that the solid conduction pathways are important in the fine plutonium dioxide powder even at higher pressures.

Also, at higher gas pressures the thermal behavior is interesting because the thermal conductivity of the powder is still changing even at pressures greater than 200 kPa. At these pressure the gas thermal conductivity is usually assumed to be in the continuum limit and, therefore, independent of pressure. Further analysis revealed that the small pore and particle sizes in the plutonium powder appear to be responsible for the pressure dependence at higher pressures.

Plutonium dioxide powder thermal conduction model

A thermal conductivity model was developed to predict the thermal behavior of this fine, highly porous powder because the experimental measurements could not be reasonably
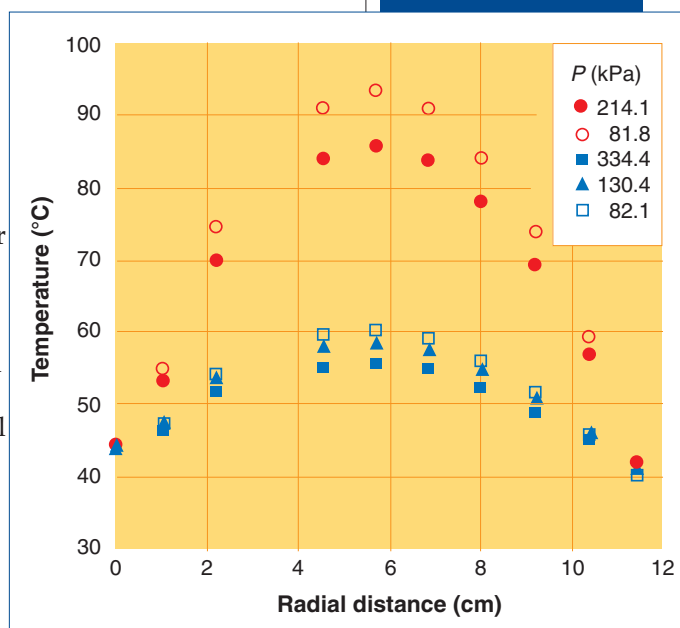
Radial temperature profiles with argon and helium as fill gases at pressures greater than 80 kilopascals. The measured pressure dependence at these conditions was unexpected. Red is argon data and blue is helium data.

MODELING AND PREDICTING
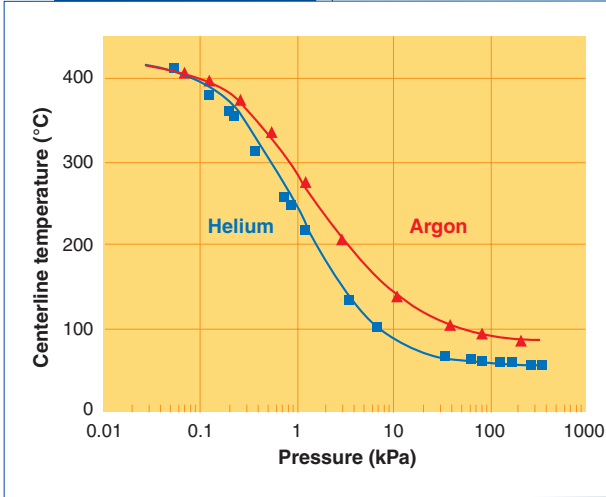
Measured centerline temperatures (indicated by points) and calculated centerline temperatures (indicated by lines) for plutonium dioxide powder with argon and helium as fill gases at different pressures. Temperatures would be similar in an ARIES container filled with calcined pure plutonium oxide powder.

interpreted using existing thermal conductivity models. The thermal conductivity expression for k_{eff} shown in the box below was derived using the powder schematic shown below it.

In this expression, k_{eff} is the effective thermal conductivity of the powder, ε is the porosity of the powder, $k_{g,o}$ is the thermal conductivity of the fill gas in the outer pore region, $k_{g,in}$ is the thermal conductivity of the fill gas in the interparticle contact fraction (L/D), k_{solid} is the thermal conductivity of the PuO_2 solid, δ is the contact roughness, and ϕ defines the solid-solid contact region in the interparticle contact fraction. The interparticle contract fraction (L/D) defines the region where conduction occurs between the solid particles across a small gap. To calculate the thermal conductivity from this expression, the porosity (ε) is experimentally measured, the gas and solid thermal conductivities are available from the literature, and the sphericity (ϕ), contact roughness (δ), and interparticle contact fraction (L/D) are fit parameters.
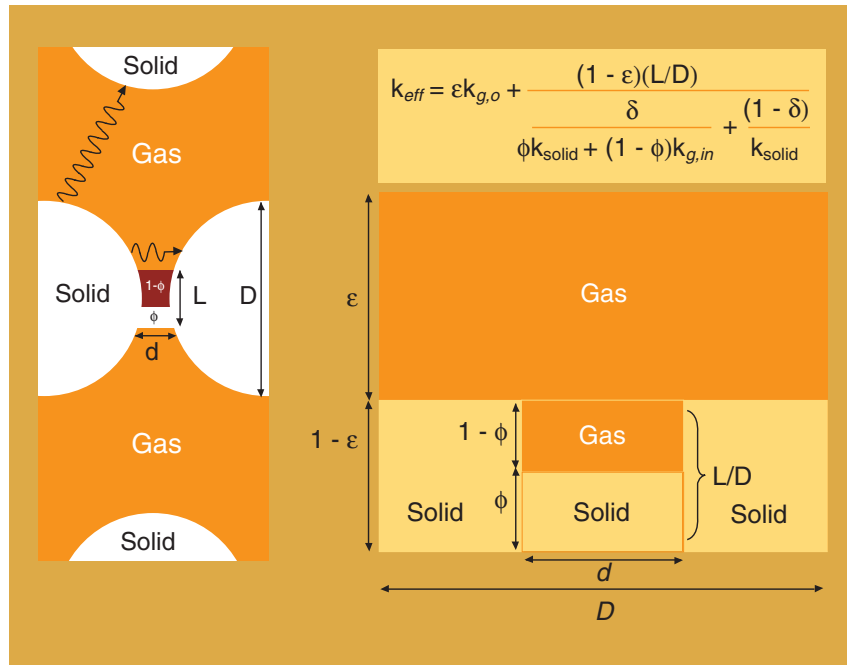
With the thermal conductivity expression in the equation to the left, the radial temperature profiles were calculated using a finite difference code that included radial and axial heat conduction, thermal radiation in the powder bed, and convection to the surrounding air as heat transfer pathways. The fit parameters for the powder were δ=0.0037, ϕ=0.00018, L/D=0.10 and the thermal radiation emissivity view factor product=0.015. Because the gas conductivity is a function

$$k_{eff} = \varepsilon k_{g,o} + \cfrac{(1 - \varepsilon)(L/D)}{\cfrac{\delta}{\phi k_{solid} + (1 - \phi)k_{g,in}} + \cfrac{(1 - \delta)}{k_{solid}}}$$

This schematic for the powder thermal conductivity model shows two parallel pathways ($\wedge\!\wedge\!\wedge\!\rightarrow$) through the gas and solid regions of the powder with the fractions determined by the powder porosity (ε). Within the solid 1-ε region, conduction occurs between the two solid particles through a small contact length, L (nondimensionalized as the parameter L/D). The relative areas of the solid-solid contact versus the solid-gas-solid contact in the interparticle contact fraction (L/D) are set by the parameter, ϕ, the sphericity. The other parameter in this model, δ, is the interparticle distance, d, divided by the total cell distance (D).

of the pore size (λ) in the free molecular region, the inner pore size (λ_{in}) of 0.68 micrometer (μm) in the contact area and the outer pore size (λ_o) of 17 μm in the outer pore region were also estimated.

The calculated centerline temperatures were in good agreement with the measured temperatures for both fill gases over the entire range of pressures. The thermal conductivity expression effectively captures that the thermal conductivities with argon and helium as fill gas approach each other at low pressures and that the thermal conductivity with argon is higher than expected at the higher pressures.

The relatively high thermal conductivity with argon as fill gas, which results in lower centerline temperatures, is important because packaging atmospheres no longer need to be strictly helium to hold centerline temperatures down. The model was able to correctly predict these data because it accounts for significant conduction through the interparticle contact area where the gases are not in the continuum limit and the argon and helium gas thermal conductivity values are much closer to each other. The model also correctly predicted the observed pressure dependence on temperature that exists at high pressures attributed to the small interparticle pore size present in these powders.

Comparison with previous plutonium dioxide powder thermal conductivity models

By using the new thermal conductivity model for the plutonium dioxide powder, we can assess the predicted thermal conductivities and centerline temperatures from the previous two studies. The earlier studies both predicted the thermal behavior of the plutonium dioxide powder in air. The new thermal conductivity model predicts that the powder conductivity is 0.15 W/(m K), compared to 0.079 W/(m K) from the Hensel study and 0.10 W/(m K)

from the Knight and Steinke study. Assuming typical packaging conditions for the storage containers from Hensel's study where the wall temperature was set equal to 173 degrees Celsius and the pressure was 3,930 kPa, we calculate the temperature profile for each set of thermal conductivity values. The temperature profiles are compared in the figure below where the predicted maximum temperature, using our new thermal conductivity expression, is 227 degrees Celsius, almost 50 degrees less than that calculated using Hensel's estimated thermal conductivity. The calculated temperature drop across the oxide bed decreases by almost half from Hensel's value of 103 degrees Celsius to our value of 55 degrees Celsius.

The wide range of the predicted temperatures between the three conductivity values demonstrates the importance of an accurate thermal conductivity value in estimating the thermal profile of storage containers with pure plutonium dioxide powder. The higher thermal conductivity predicted in our current study that results in a lower temperature profile will also lead to a lower estimate of the container pressure, since one of the effects of increased temperatures in the container is expansion of the fill gas and subsequent pressure increase. Because our thermal conductivity value is derived from plutonium powder data, these predictions provide a more accurate estimate of the temperatures and pressures in 3013 storage containers.

Predicted oxide temperature profiles in a storage container with air as a fill gas at a pressure of 3,930 kilopascals and at a wall temperature of 173 degrees Celsius The thermal conductivities from studies by Hensel (1998) and Knight and Steinke (1997) along with the predicted thermal conductivity from the current study were used to calculate the temperature profiles.
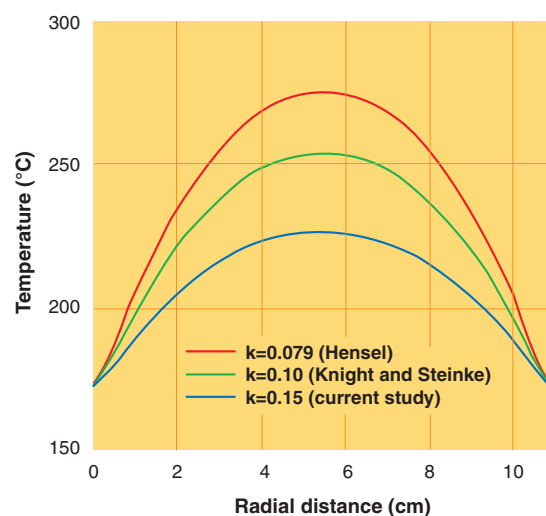
The physics and chemistry of oxidation
Defining the electronic structure of surface oxides

This article was contributed by Martin Butterfield, Los Alamos Neutron Science Center; Tomasz Durakiewicz, Materials Science and Technology Division; and Richard Martin, Theoretical Division.

Contributors to the experiment include Martin Butterfield, Los Alamos Neutron Science Center; John Joyce, Elzbieta Guziewicz, Aloysius Arko, and Kevin S. Graham, Materials Science and Technology Division; and David P. Moore and Luis Morales, Nuclear Materials Technology Division.

Contributors to theory include Ionut Prodan, José Sordo, Konstantin Kudin, and Gustavo Scuseria, Rice University, Houston.

Understanding the physics and chemistry of oxidation is essential for long-term plutonium storage. Under normal atmospheric conditions oxide layers cover plutonium metal surfaces, which ultimately control chemical reactivity. Our experimental and theoretical efforts are aimed at revealing the electronic structure of surface oxides as well as the mechanisms of their formation. First, we describe the manner in which plutonium oxides develop in a highly controlled environment as seen by photoemission. We also describe this evolution using theoretical ab initio calculations of the electronic structure.

Photoemission spectroscopy (PES) provides an excellent direct probe of the electronic structure of surfaces and is extremely sensitive to surface contaminants so that even fractions of monolayers of adsorbed gases can be detected. Typical excitation sources include specific helium (He) plasma emission lines: He Iα, 21.2 electronvolts (eV); He IIα, 40.8 eV; and He IIβ, 48.4 eV. Alternatively tunable sources in the vacuum ultraviolet (UV) region, such as those at synchrotron sources, have also been used. Los Alamos' Laser Plasma Light Source (LPLS) project has also provided tunable, high-intensity excitation light for PES studies.

We conducted our studies of the surface electronic structure following gas adsorption using the He IIα 40.8-eV excitation energy because at that energy there is a sizeable cross section for both oxygen 2p and plutonium 5f and 6d electronic shells. Because of sensitivity to trace impurities, the sample was kept at a base pressure of 6×10^{-11} torr during and following cleaning by laser ablation. Laser ablation has proven to be an excellent way to remove surface contaminants from actinides and other materials. The low base pressure ensures that any residual background adsorption of trace gases from the vacuum does not compromise the measurements over an extended timescale (hours).

The figure above shows PES data for a "clean" δ-plutonium surface and a plutonium surface with a small residual amount of oxygen. A difference spectrum between the two is provided and has the spectral
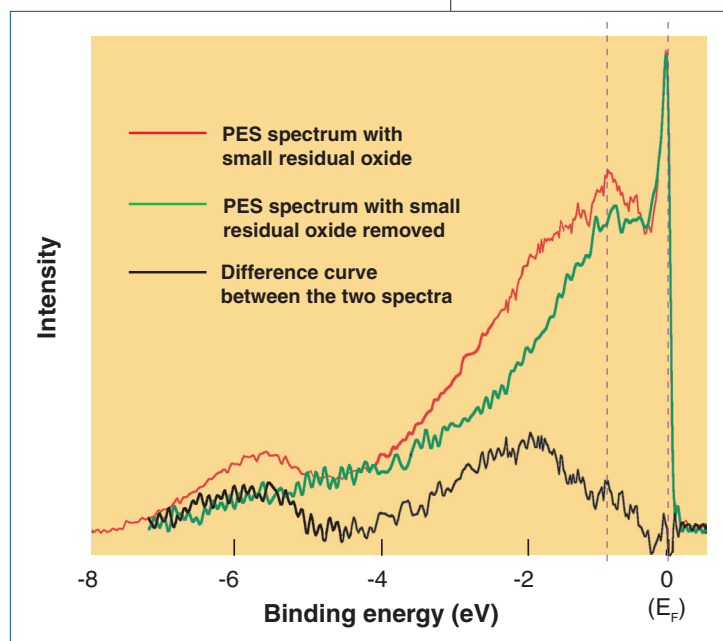
Clean and "nearly" clean δ-plutonium along with the difference spectrum between the

Top: This view through a window on the side of the measurement chamber shows the copper sample holder, which is a central part of the apparatus. Samples mounted to the holder may be cooled to 10 kelvin for photoemission measurements.

Center: A close-up of the sample holder. The small square in the center is the plutonium sample. Surface cleaning is performed by focusing an infrared (1,064-nanometer) laser beam on the sample.

Bottom: The photoemission measurement chamber. The top and middle photos were taken through the inspection window in the front of the chamber. Pressure inside the chamber is approximately 10^{13} times lower than atmospheric pressure outside the chamber. To maintain such a high-vacuum environment, the chamber must occasionally be heated to temperatures above 120 degrees Celsius. The chamber is wrapped in aluminium foil to ensure uniform temperature distribution and thermal insulation during bakeout to establish operational pressure.
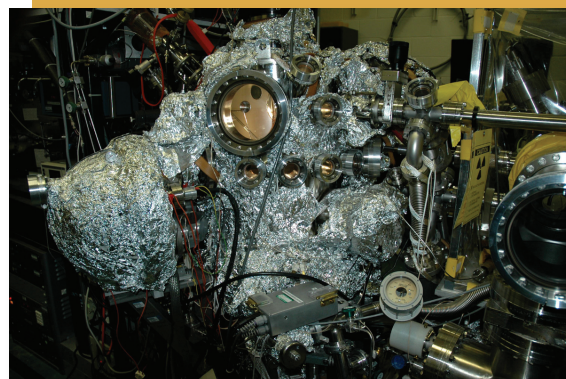
Photos by
Tomasz Durakiewicz and
Ela Guziewicz

characteristics of Pu_2O_3. The figure also demonstrates the need to obtain as clean a surface as possible to determine the true electronic structure of the base metal. The clean surface exhibits two main features typical of δ-plutonium: a localized peak at about 1 eV attributed to emission from the 5f level and characteristics at the Fermi level attributed to emission from 5f and conduction electrons. The subtle distinctions in features inherent to these clean surfaces can become obscured by trace contamination. In fact, earlier investigations on δ-plutonium sample surfaces purported to be "clean" exhibit low-level oxide contamination that may be comparable to our low-level doses.

Gas dosing was carried out by means of a needle valve from a gas line into the main vacuum chamber, which allowed for accurate surface exposures for O_2 gas measured in langmuirs (L). (A langmuir is a unit of measure used in surface science that is roughly equivalent to producing a surface saturated monolayer with a physically or chemically adsorbed species provided all incident gas molecules react and remain on the surface with unity probability.)

Given the reactive nature of plutonium and other actinides, this places a significant burden on the experimentalist's ability to work at an atmosphere where the surface is not compromised by spurious nondesirable adsorption. From the kinetic theory of gases, a 1-langmuir exposure is equivalent to 10^{-6} torr gas pressure for one second at the surface. In this work measurements were made at temperatures of 10, 77, and 300 kelvin (K) to assess the relative role of kinetic formation and transformation rates among the plutonium oxides.

The figure on this page demonstrates the changes in surface electronic structure following sequential gas exposures at 77 K with 1, 5, 10, and 20 langmuirs of O_2. Following a 1-langmuir O_2 exposure an oxide is formed that we associate with Pu_2O_3 at the metal surface. In spectra recorded following a 5-langmuir O_2 exposure there is a superposition of two oxides, which we designate as Pu_2O_3 and PuO_2. The presence of two oxides is indicated by four peaks at approximately 1.6 and 5.5 eV (Pu_2O_3) and at 2.5 and 4.6 eV (PuO_2). Plutonium-related features, primarily 5f in character with some 6d, appear in the 0–3 eV energy interval, while oxygen features attributed to emission from 2p atomic levels appear in the 4–8 eV energy range.

Further O_2 exposure causes the gradual disappearance of the Pu_2O_3 peaks and the gradual growth of the PuO_2 peaks. This suggests that the PuO_2 is in fact growing on top of the initial Pu_2O_3 layer, and even following an exposure of 20 langmuirs there is still some evidence of a residual Pu_2O_3 component. When the sample
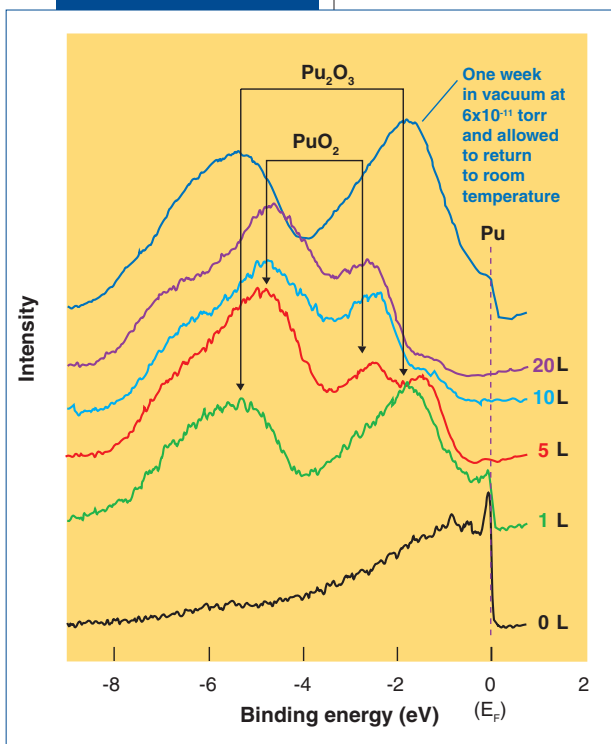
Results of gas dosing of the δ-plutonium surface with oxygen (O_2) at 77 kelvin.

was allowed to recover to room temperature and left undisturbed in a vacuum of $6x10^{-11}$ torr for one week, it appears that all of the oxide within the PES probe depth may have converted to Pu_2O_3. However, a Fermi edge (E_F) reappeared following this latest reaction period in vacuum. This could also suggest that rather than a conversion of the oxide, the oxygen on the surface has either desorbed into the vacuum (not probable given the extremely high affinity of plutonium for oxygen) or diffused into the metal leaving only a thin Pu_2O_3 oxide layer (between 1 and 5 langmuirs) at the surface. It is also possible that the reduction
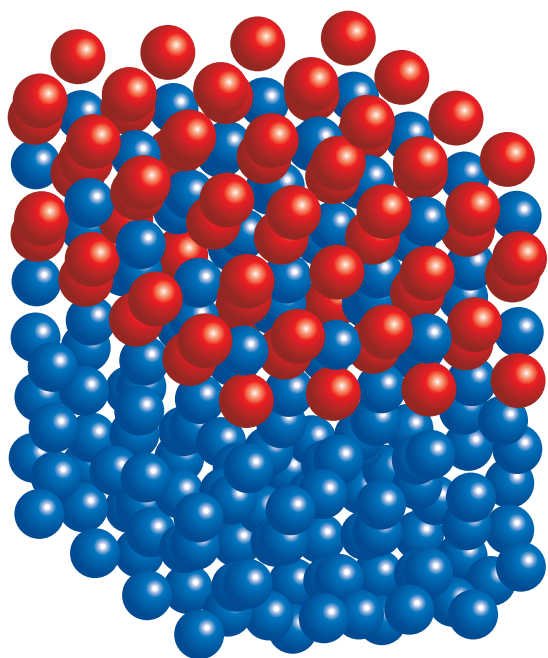
Oxidation of plutonium metal showing growth of a Pu_2O_3 overlayer. Plutonium atoms are shown in blue and oxygen atoms shown in red. The base plutonium metal is shown as a polycrystalline solid.

to Pu_2O_3 resulted in the formation of oxide islands on the surface, therefore exposing areas of the metal substrate within our probe depth and resulting in spectral intensity at the Fermi edge.

PES results following O_2 gas dosing at a temperature of 77 K support an idealized model for the formation of Pu_2O_3 at the δ-plutonium metal surface with subsequent PuO_2 formation on the initial oxide. This is schematically indicated by the development and growth of an oxide layer on top of plutonium metal. Holding the sample at room temperature in a vacuum for an extended period of time (ten hours or more), results in the remaining surface oxide eventually converting to Pu_2O_3. The reappearance of a Fermi edge in the data after the sample was left in vacuum for one week and allowed to warm up to room temperature suggests that the oxygen at the sample surface diffused into the sample.

It is also possible that the reduction of the oxide caused island growth; thereby exposing some of the metal surface within the PES probe depth. The PuO_2 data at 77 K and the Pu_2O_3 at 300 K both demonstrate that these oxides are insulators with no photoemission intensity at the Fermi edge. Our previous PES results for O_2 gas dosing at room temperature support a model in which a Pu_2O_3 is formed immediately at the metal surface and persists with increasing exposure.

These systems have been studied theoretically using a new generation of density

functional theory (DFT) termed hybrid DFT. The details of these approaches are beyond the scope of this article but basically involve combining the exact, nonlocal, Hartree-Fock exchange interaction with the traditional local density approximation (LDA) or generalized gradient approximation (GGA) and correlation interactions of density functional theory.

In their initial use, hybrid functionals were designed and mathematically constructed to faithfully predict the heats of formation of a set of small molecules, e.g. hydrogen (H_2), carbon

The total density of states for the PuO_2 and Pu_2O_3 ferromagnetic states computed in the PBEO approximation (black) compared with experiment (red).

dioxide (CO_2), ammonia (NH_3), water (H_2O), etc., but researchers quickly discovered that they performed quite well outside this set. In particular, they provide excellent bond energies and properties for molecules containing transition metal and actinide centers. These hybrid functionals have had a dramatic impact in molecular quantum chemistry. They have significantly improved our predictive capability for bond energies, our ability to predict reaction barriers and understand mechanisms, and our ability to predict excitation energies and oscillator strengths in molecules via linear response theory.

Only recently have they been applied to solids with full periodic boundary conditions. Preliminary results suggest they largely remedy two long-standing failures of conventional density functional theory: the prediction of metallic versus insulating behavior in the class of materials known as Mott insulators and the systematic underestimation of the band gap in semiconductors and insulators.

The calculations for UO_2, Pu_2O_3, and PuO_2 using the hybrid DFT provides a substantive improvement in the current state-of-the-art for calculating insulating actinide materials. Within the framework of the hybrid DFT we realize the desirable solution of an insulator for all three materials.

The UO_2 and Pu_2O_3 magnetic solutions are also in agreement with experiment. While the antiferromagnetic solution for PuO_2 in the hybrid DFT is not evident from the available susceptibility and neutron data, it has been suggested that the discrepancy between the low-lying states observed in the neutron scattering data and the temperature dependence of the susceptibility can be understood in terms of an antiferromagnetic interaction between the metal sites. We believe this
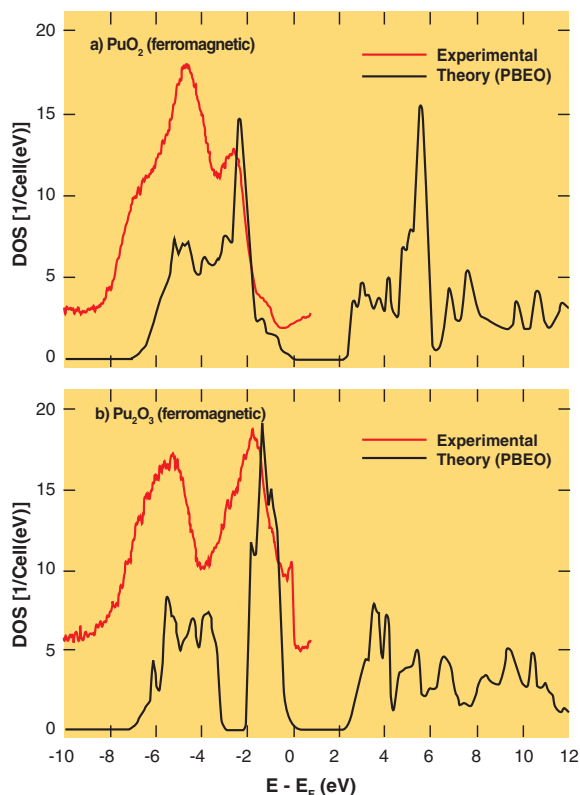
common framework from which to compute and compare insulating actinide oxides provides a significant step forward in the understanding of these materials.

These improvements are of paramount importance for the study of actinide oxides because the conventional density functional theory approaches predict them to be metals, when in fact they are insulators with significant band gaps. On the other hand, we recently reported the first implementation of hybrid density functional theory capable of describing periodic solids containing *f*-elements and applied it successfully to the electronic structure of uranium dioxide (UO_2). This approach correctly predicted the anti-ferromagnetic, insulating ground state observed experimentally. In contrast, conventional LDA and GGA approaches both find a ferromagnetic, metallic ground state. The band gap, lattice constant, bulk modulus, photoemission spectrum, and optical spectrum were all in good agreement with experiment. Encouraged by this, we have extended this study to PuO_2 and Pu_2O_3.

In the ionic limit, formal charges for plutonium in PuO_2 and Pu_2O_3 are +4 and +3, respectively, corresponding to formal populations of f^4 and f^5. These configurations lead to local S=2 and S=5/2 plutonium moments, which can couple with other sites in either a ferromagnetic or anti-ferromagnetic manner. We find the anti-ferromagnetic solution to be the ground state in either case. However, the magnetic coupling is relatively weak and, aside from the energy, most properties are identical between the two states. In what follows, we therefore focus on the ferromagnetic solution.

The lattice constant of PuO_2 is predicted to be 5.39 angstroms (Å), which is in agreement with the experimental result of 5.40 Å. The unpaired spin density on the plutonium center is similar to the estimate from the ionic limit,
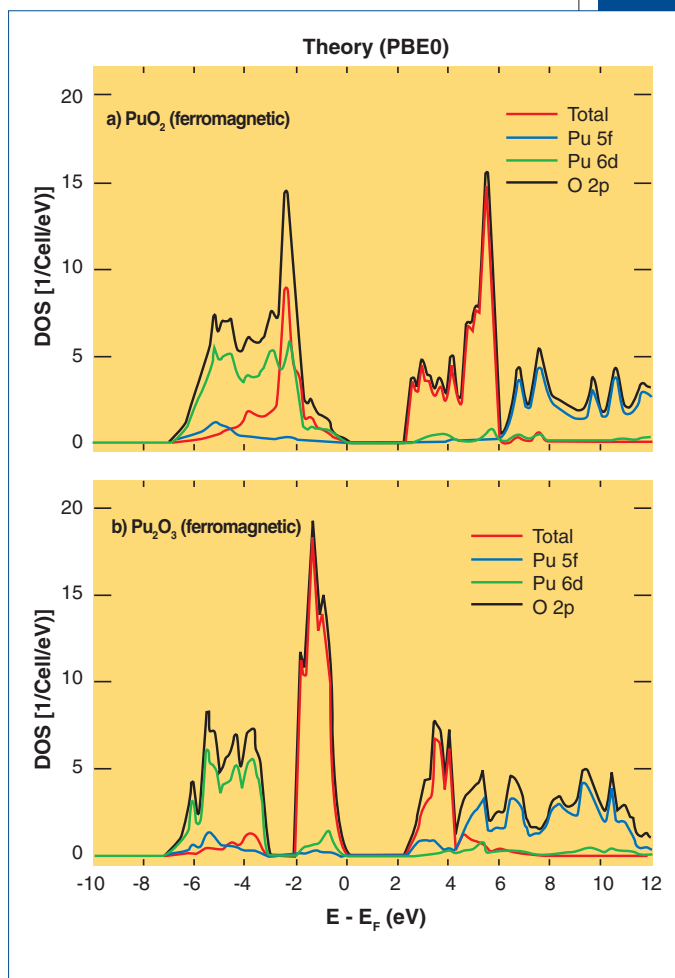
The partial density of states for the PuO_2 and Pu_2O_3 ferromagnetic states computed in the PBE0 approximation. Note that both oxygen 2p and plutonium 5f orbitals contribute significantly to the levels near the Fermi energy in PuO_2, implying significant mixing. By way of contrast, the peak near E_F in Pu_2O_3 is predominantly plutonium 5f, with much less oxygen 2p character.

Defining the Electronic Stucture

For further reading:

"Surface Chemistry of Pu Oxides," J.D. Farr, R.K. Schulze, and M.P. Neu, Journal of Nuclear Materials, 328 (2-3), 124-136, 2004.

"Photoemission of Surface Oxides and Hydrides of Delta Plutonium," M.T. Butterfield, T. Durakiewicz, E. Guziewicz, J.J. Joyce, A.J. Arko, K.S. Graham, D.P. Moore, D. P., and L.A. Morales, Surface Science, 571 (1-3), 74-82, 2004.

"Hybrid Density-Functional Theory and the Insulating Gap of UO_2," Konstantin N. Kudin, Gustavo E. Scuseria, and Richard L. Martin, Physical Review Letters 89(26), 266402/1-266402/4, 2002.

yielding 4.1 and 5.1 electrons for PuO_2 and Pu_2O_3, respectively. Both actinide oxides are predicted to be insulators, with gaps of 2.4 and 2.5 eV, respectively.

The theoretical PuO_2 photoemission spectrum shows a weak feature near the Fermi edge followed by a strong peak at about 2.5 eV and a weaker one near 4.5 eV. It is encouraging that these peak positions are in good agreement with the experiment. There is, however, an additional feature near 6 eV is observed in the experiment, but is absent in the calculation. In addition, the relative intensity of the 2.5- and 4.5 eV peaks is not well reproduced by the calculation. It should also be noted that we have implicitly assumed identical photoemission cross sections for the oxygen 2p and uranium 5f orbitals in making this comparison. At 40.8 eV incident photon energy, the intensity ratio of the oxygen 2p photoemission peak to the plutonium 5f photoemission peak of approximately 1.5 is probably more appropriate. This adjustment would tend to increase the intensity of the 4.5 eV peak, but not sufficiently to make it stronger than the low-energy one.

For Pu_2O_3, the peak near the Fermi edge is principally plutonium 5f in character and the higher binding energy feature is mostly oxygen 2p. This spectrum is similar to that of UO_2, which also exhibits two distinct peaks of mostly uranium 5f and oxygen 2p parentage. On the other hand, the region near the Fermi edge in PuO_2 is nearly a 50:50 mixture of plutonium 5f and oxygen 2p, signifying much greater metal-ligand mixing.

This is a surprising result, given the smaller overlap anticipated in plutonium because of the smaller radius of the plutonium 5f orbital. In addition to the reduction in 5f radius in going from uranium to plutonium, one expects a stabilization of the plutonium 5f site orbital energy. In perturbation theory, the mixing between two levels is effectively given by the overlap integral divided by the difference in site energies. It may be that the origin of the stronger mixing is related to the stabilization of the plutonium 5f orbital and an unanticipated degeneracy with the oxygen 2p level. In this hypothesis, the small mixing in the Pu_2O_3 spectrum would be associated with the higher plutonium 5f site energy expected in the less highly charged, formally Pu^{3+}, ion.

While there is clearly much to be done, we are encouraged by the argument between theory and experiment and believe the combination will tell us much about the electronic structure of these complex systems.

Density functional theory

Density functional theory (DFT) is one of the most popular and successful quantum mechanical approaches to the many-body electronic structure calculations of molecular and condensed matter systems. Within the framework of DFT, the practically unsolvable many-body problem of interacting electrons is reduced to a solvable problem of a single electron moving in an averaged effective force field. This effective force field can be represented by a potential energy being created by all the other electrons as well as the atomic nuclei, which are seen as fixed in terms of the Born-Oppenheimer approximation.

Description of the Theory

In contrast to traditional methods like Hartree-Fock theory which are based on the complicated many-electron wavefunction DFT is written in terms of the electron density, giving this theory its name. DFT is an exact theory only for the free electron gas, while for the treatment of extended atomic systems various approximations have to be made. In many cases DFT gives quite satisfactory results in comparison to experimental data at relatively low computational costs when compared to other ways of solving the quantum mechanical many-body problem.

DFT has been very popular for calculations in solid state physics since the 1970s. However, it was not considered accurate enough for calculations in quantum chemistry until the 1990s, when the approximations used in the theory were greatly refined. DFT is now the leading method for electronic structure calculations in both fields. However, there are still systems which are not described very well by DFT. One famous example is the false prediction of the band gap in semi-conductors. The method also fails to describe properly intermolecular interactions, especially van der Waals forces (dispersion).

Early Models

The first true density functional theory was developed by Thomas and Fermi in the 1920s. They calculated the energy of an atom by representing its kinetic energy as a functional of the electron density, combining this with the classical expressions for the nuclear-electron and electron-electron interactions (which can both also be represented in terms of the electron density).

Although this was an important first step, the Thomas-Fermi equation's accuracy was limited because it did not attempt to represent the exchange energy of an atom predicted by Hartree-Fock theory. An exchange energy functional was added by Dirac in 1928.

However, the Thomas-Fermi-Dirac theory remained rather inaccurate for most applications because it is difficult to represent kinetic energy with a density functional, and it neglects electron correlation entirely.

Derivation and Formalism

As usual in many-body electronic structure calculations, the nuclei of the treated molecules or clusters are seen as fixed (Born-Oppenheimer approximation), generating a static external potential V in which the electrons are moving. A stationary electronic state is then described by a wave function $\Psi(\vec{r}_1, ..., \vec{r}_N)$ fulfilling the many-electron Schrödinger equation

$$H\Psi = [T + V + U]\,\Psi = \left[\sum_i^N -\frac{\hbar^2}{2m}\nabla_i^2 + \sum_i^N V(\vec{r}_i) + \sum_{i<j} U(\vec{r}_i, \vec{r}_j)\right]\Psi = E\Psi$$

where N is the number of electrons and U is the electron-electron interaction. The operators T and U are so-called universal operators as they are the same for any system, while V is system dependent or non-universal. As one can see the actual difference between a single-particle problem and the much more complicated many-particle problem just arises from the interaction term U. Now, there are many sophisticated methods for solving the many-body Schrödinger equation, e.g. there is diagrammatic perturbation theory in physics, while in quantum chemistry one often uses configuration interaction (CI) methods, based on the systematic expansion of the wave function in Slater determinants. However, the problem with these methods is the huge computational effort, which makes it virtually impossible to apply them efficiently to larger complex systems.

Here DFT provides an appealing alternative, being much more versatile as it provides a way to systematically map the many-body problem, with U, onto a single-body problem without U. In DFT the key variable is the particle density $n(\vec{r})$ which is given by

$$n(\vec{r}) = N \int \mathrm{d}^3 r_2 \int \mathrm{d}^3 r_3 ... \int \mathrm{d}^3 r_N \Psi^*(\vec{r}, \vec{r}_2, ..., \vec{r}_N)\Psi(\vec{r}, \vec{r}_2, ..., \vec{r}_N)$$

Hohenberg and Kohn proved in 1964 [1] that the relation expressed above can be reversed, i.e. to a given ground state density $n_0(\vec{r})$ it is in principle possible to calculate the corresponding ground state wave function $\Psi_0(\vec{r}_1, ..., \vec{r}_N)$. In other words, Ψ_0 is a unique functional of n_0, i.e. $\Psi_0 = \Psi_0[n_0]$ and consequently all other ground state observables O are also functionals of n_0 $\langle O\rangle[n_0] = \langle\Psi_0[n_0]|O|\Psi_0[n_0]\rangle$
From this follows in particular, that also the ground state energy is a functional of n_0 $E_0 = E[n_0] = \langle\Psi_0[n_0]|T + V + U|\Psi_0[n_0]\rangle$, where the contribution of the external potential $\langle\Psi_0[n_0]|V|\Psi_0[n_0]\rangle$ can be written explicitly in terms of the density $V[n] = \int V(\vec{r})n(\vec{r})\mathrm{d}^3$.

The functionals $T[n]$ and $U[n]$ are called universal functionals while $V[n]$ is obviously non-universal, as it depends on the system under study. Having specified a system, i.e. V is known, one then has to minimise the functional

$$E[n] = T[n] + U[n] + \int V(\vec{r})n(\vec{r})\mathrm{d}^3 r$$

with respect to $n(\vec{r})$, assuming one has got reliable expressions for $T[n]$ and $U[n]$.

A successful minimisation of the energy functional will yield the ground state density n_0 and thus all other ground state observables.

The variational problem of minimising the energy functional $E[n]$ can be solved by applying the Lagrangian method of undetermined multipliers, which was done by Kohn and Sham in 1965 [2]. Hereby, one uses the fact that the functional in the equation above can be written as a fictitious density functional of a non-interacting system

$$E_s[n] = \langle \Psi_s[n] | T_s + V_s | \Psi_s[n] \rangle ,$$

where T_s denotes the non-interacting kinetic energy and V_s is an external effective potential in which the particles are moving. Obviously, $n_s(\vec{r}) \equiv n(\vec{r})$ if V_s is chosen to be

$$V_s = V + U + (T_s - T) .$$

Thus, one can solve the so-called Kohn-Sham equations of this auxiliary non-interacting system

$$\left[-\frac{\hbar^2}{2m} \nabla^2 + V_s(\vec{r}) \right] \phi_i(\vec{r}) = \epsilon_i \phi(\vec{r}) ,$$

which yields the orbitals ϕ_i that reproduce the density $n(\vec{r})$ of the original many-body system

$$n(\vec{r}) \equiv n_s(\vec{r}) = \sum_i^N |\phi_i(\vec{r})|^2 .$$

The effective single-particle potential V_s can be written in more detail as

$$V_s = V + \int \frac{e^2 n_s(\vec{r}')}{|\vec{r} - \vec{r}'|} d^3 r' + V_{XC}[n_s(\vec{r})] ,$$

where the second term denotes the so-called Hartree term describing the electron-electron Coulomb repulsion, while the last term V_{XC} is called exchange correlation potential. Here, V_{XC} includes all the many particle interactions. Since the Hartree term and V_{XC} depend on $n(\vec{r})$, which depends on the ϕ_i, which in turn depend on V_s, the problem of solving the Kohn-Sham equation has to be done in a self-consistent way. Usually one starts with an initial guess for, then one calculates the corresponding V_s and solves the Kohn-Sham equations for the ϕ_i. From these one calculates a new density and starts again. This procedure is then repeated until convergence is reached.

Approximations

The major problem with DFT is that the exact functionals for exchange and correlation are not known except for the free electron gas. However, approximations exist which permit the calculation of certain physical quantities quite accurately. The most widely used approximation is the local density approximation (LDA), where the functional depends only on the density at the coordinate where the functional is evaluated. Generalized gradient approximations (GGA) are still local but also take into account the gradient of the density at the same coordinate. Using the latter (GGA) very good results for molecular geometries and ground state energies have been achieved. Many further incremental improvements have been made to DFT by developing better representations of the functionals.

Relativistic Generalization

The relativistic generalization of the DFT formalism leads to a current density functional theory.

Applications

In practice, Kohn-Sham theory can be applied in two distinct ways depending on what is being investigated. In the solid state, plane wave basis sets are used with periodic boundary conditions. Moreover, great emphasis is placed upon remaining consistent with the idealised model of a 'uniform electron gas', which exhibits similar behaviour to an infinite solid. In the gas and liquid phases, this emphasis is relaxed somewhat, as the uniform electron gas is a poor model for the behaviour of discrete atoms and molecules. Because of the relaxed constraints, a huge variety of exchange-correlation functionals have been developed for chemical applications. The most famous and popular of these is known as B3LYP [3-5]. The adjustable parameters of these functionals are generally fitted to a 'training set' of molecules. Unfortunately, although the results obtained with these functionals are usually relatively accurate for most applications, there is no systematic way of improving them (in contrast to some of the traditional wavefunction-based methods like configuration interaction or coupled cluster method). Hence, in the current DFT approach it is not possible to estimate the error of the calculations without comparing them to other methods or experiment.

References
[1] P. Hohenberg and W. Kohn, Phys. Rev. 136 (1964) B864
[2] W. Kohn and L. J. Sham, Phys. Rev. 140 (1965) A1133
[3] A. D. Becke, J. Chem. Phys. 38 (1998) 3089
[4] C. Lee, W. Yang, and R. G. Parr, Phys. Rev. B 37 (1988) 785
[5] P. J. Stephens, F. J. Devlin, C. F. Chabalowski, and M. J. Frisch, J. Phys. Chem. 98 (1994) 11623

*—This article was taken from Wikipedia, the free encyclopedia
http://en.wikipedia.org/wiki/Density_functional_theory*

Actinide Research Quarterly
is produced by Los Alamos
National Laboratory

About the Quarterly

Actinide Research Quarterly
highlights recent achievements and
ongoing programs of the Nuclear
Materials Technology (NMT) Division.
We welcome your suggestions and
contributions. ARQ can be read on
the World Wide Web at:

www.lanl.gov/arq

Address correspondence to
Actinide Research Quarterly
c/o Meredith Coonley
Mail Stop E500
Los Alamos
National Laboratory
Los Alamos, NM 87545

If you have questions, comments, suggestions,
or contributions, please contact the ARQ staff at
arq@lanl.gov.

Phone (505) 667-0392
Fax (505) 665-7895